ELSEVIER

Journal of Chromatography A, 702 (1995) 125–142

JOURNAL OF CHROMATOGRAPHY A

Modeling non-linear elution of proteins in ion-exchange chromatography

Stuart R. Gallant, Amitava Kundu, Steven M. Cramer*

Howard P. Isermann Department of Chemical Engineering, Rensselaer Polytechnic Institute, Troy, NY 12180, USA

Abstract

The problem of non-linear elution of a band of protein in isocratic ion-exchange chromatography leads to a pair of coupled non-linear partial differential equations. The equilibrium may be modeled using the Steric Mass Action (SMA) model of ion exchange, which treats both the salt dependence of protein adsorption and the steric shielding present under non-linear conditions. Neglecting axial dispersion, a model of ideal chromatography is formulated that may be solved by the method of characteristics. The predictions of this relatively simple model are shown to agree with experimental results concerning the non-linear elution of cytochrome *c* in a strong cation-exchange column. Of particular interest is the existence of two plateaus in the solution of this problem for large injection volumes. While this result cannot be understood or predicted on the basis of the traditional Langmuir isotherm or other currently available descriptions of adsorption, the chromatographic model presented in this work makes this otherwise anomalous result clear. Further, the use of such a model during parameter estimation is discussed.

1. Introduction

Multi-component isotherms play a crucial role in determining the behavior of non-linear chromatographic systems [1]. When combined with an appropriate description of the transport through the column, a reliable multi-component isotherm makes it possible to predict the chromatographic elution times and band shapes of components in the chromatographic system. Two important effects dictated by isotherm shape are the formation self-sharpening fronts or "shocks" and the formation of rarefaction waves or "tails."

Because of the central importance of multi-component isotherms to the understanding of chromatographic behavior, the last decade has been a renaissance in the study of multi-component isotherms in liquid chromatography [2]. Researchers have investigated and attempted to describe equilibrium adsorption behavior on a wide variety of stationary phase surface chemistries. In this paper, the focus of concern will be the representation of the equilibrium adsorption of a single protein and a counter ion on an ion-exchange surface.

The problem which is investigated, the injection of a chromatographic band of finite width and concentration, has been discussed previously for the Langmuir isotherm [3,4]. Some readers might feel that this is a relatively well understood problem; however, careful examination of the experiments and simulations presented below demonstrates some novel observations about this problem. In particular, the existence of a two-plateau band shape that has not previously been

* Corresponding author.

0021-9673/95/$09.50
SSDI 0021-9673(94)00992-9

presented in the literature is predicted by the theoretical treatment and documented by experiment. Further, it is our purpose in this paper to conduct a test of two models of ion-exchange adsorption: The Steric Mass Action (SMA) and Stoichiometric Displacement/Electroneutrality (SDM/Electroneutrality) models. The ability of SMA, SDM/Electroneutrality and a modifier-dependent Langmuir isotherm to represent protein isotherms is evaluated in the Appendix.

Although the model presented here would not apply to cases in which more than one protein was present, it should be clear that implementation of the Steric Mass Action isotherm in a more sophisticated model of mass transport would have wide application for multi-component separations in isocratic, gradient and displacement modes. Our research group has employed this isotherm extensively in the study of displacement chromatography, and new work will be published in the near future on modeling non-linear gradient chromatography.

2. Theory

2.1. Background

A number of researchers have suggested techniques for modeling protein adsorption in ion-exchange chromatography under conditions of varying salt concentration. Boardman and Partridge [5] observed that the retention of proteins in cation-exchange chromatography under dilute conditions could be described using a relatively simple exponential expression. Using the notation employed below, that relationship may be stated as

$$k'_i = \beta \cdot \left(\frac{Q_i}{C_i}\right) = \beta K_{1i} \cdot \left(\frac{\Lambda}{C_1}\right)^{\nu_i} \quad (1)$$

where k'_i is the capacity factor, β is the phase ratio, Q_i is the concentration of bound protein, C_i is the mobile phase protein concentration, K_{1i} is the equilibrium constant of the exchange reaction, Λ is the bed capacity, C_1 is the salt concentration and ν_i is the protein's characteristic charge. Regnier and co-workers [6,7] have employed this model, the Stoichiometric Displacement Model or SDM, in order to predict protein retention in analytical chromatography.

This exchange reaction-based approach has been extended to modeling the adsorption from concentrated protein solutions [8,9]. In preparative chromatography, the concentration of protein adsorbed on the stationary phase will often represent a large fraction of the total bed capacity Λ. In order to represent the limited capacity of the stationary phase, the electroneutrality condition is invoked:

$$\Lambda = Q_1 + \sum_{i=2}^{NC} \nu_i Q_i \quad (2)$$

where Q_1 represents the concentration of salt counter ions bound to the stationary phase, Q_i represents the concentration of the ith component bound to the stationary phase and NC is the number of components in the mobile phase. Utilizing Eq. 2 to represent the finite capacity of the stationary phase, a group of non-linear equations which define the bound concentration of each adsorbed component as a function of the mobile phase concentrations is formulated [10]:

$$Q_i = F_i(C_1, C_2, \ldots, C_{NC}) \quad i = 1, \ldots, NC \quad (3)$$

where the system of non-linear equations F_i may be solved using a Newton–Raphson technique. Combination of these functions with the appropriate mass balances on the adsorbed species in the mobile and stationary phases allows the calculation of simulated chromatograms [8,11]. This type of model will be referred to as the SDM/electroneutrality model below.

As pointed out by Velayudhan [12], the use of the electroneutrality condition may be too loose a restriction on the binding capacity of a chromatographic column for proteins and large polyelectrolytes. Large molecules such as proteins can sterically block substantially more ion-exchange sites than they interact with. Fortunately, as will be shown below, this steric effect may be accounted for by replacing Eq. 2 with a more restrictive condition. The resulting model has been designated the Steric Mass Action (SMA) ion-exchange formalism [13].

2.2. Steric mass action formalism

The Steric Mass Action (SMA) formalism is a three-parameter model of ion exchange designed specifically for representation of multi-component protein–salt equilibrium in ion-exchange chromatography. In the case of a solution dilute in protein, it reduces to the model originally proposed by Boardman and Partridge [5]. However, as the concentration of protein bound to the stationary phase rises, the model takes into account the effect of steric shielding on the capacity of the stationary phase. As a result, it is capable of predicting the multi-component adsorption of protein under dilute and concentrated conditions.

Fig. 1 depicts the equilibrium adsorption of a protein from an aqueous salt solution on to an ion-exchange surface. The protein is bound to the stationary phase at a number of exchange sites given by its characteristic charge, ν_i. As can be seen, a number of sites are not occupied by the protein. In order to maintain of electroneutrality, counter ions will be bound to these sites, some of which may be sterically shielded by the protein. As a result, the sterically shielded sites will be unavailable for exchange as long as this protein remains bound to the surface. The SMA formalism represents this adsorption process as a stoichiometric exchange of mobile phase protein and bound counter ions [13]:

$$C_i + \nu_i \bar{Q}_1 \Leftrightarrow Q_i + \nu_i C_1 \quad i = 2, \ldots, NC \tag{4}$$

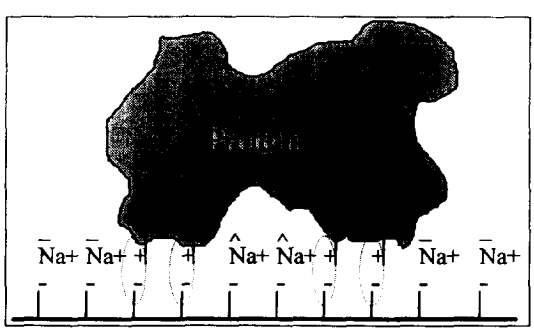

Fig. 1. Schematic diagram of protein binding on a cation-exchange surface (Brooks 1992). Na$^+$ represents the counter ions, in this case sodium ions. $\hat{\text{Na}}^+$ represents the counter ions sterically shielded by the protein.

where C_i and Q_i refer to the concentration of protein in the mobile phase and on the stationary phase, C_1 refers to the concentration of salt in the mobile phase and $\bar{Q}_1$ refers to the concentration of bound salt available for exchange. The equilibrium constant of the reaction may be written as

$$K_{1i} = \left(\frac{Q_i}{C_i}\right)\left(\frac{C_1}{\bar{Q}_1}\right)^{\nu_i} \quad i = 2, \ldots, NC \tag{5}$$

The term "salt" is used generically throughout what follows; however, the reader should bear in mind that what is being discussed are monovalent cations (in cation-exchange chromatography) or anions (in anion-exchange chromatography). For example, in the experiments and simulations below, the protein employed, cytochrome *c*, has a positive characteristic charge, as does the monovalent cation with which it exchanges, sodium.

Each protein molecule may sterically shield some salt counter ions on the adsorptive surface. The amount of salt counter ions blocked by a particular protein will be proportional to the concentration of that protein on the surface:

$$\hat{Q}_{1i} = \sigma_i Q_i \quad i = 2, \ldots, NC \tag{6}$$

Electroneutrality requires that

$$\Lambda = \bar{Q}_1 + \sum_{i=2}^{NC} (\nu_i + \sigma_i) Q_i \tag{7}$$

Having introduced the SMA equations, a word about the meaning of the steric factor is necessary. In ion-exchange chromatography, non-idealities will be present in the mobile and stationary phases. Of course, these non-idealities may be accounted for by the use of activity coefficients. However, as one of the dominant sources of non-ideality is the differences in relative size of the adsorbed components, as suggested originally by Velayudhan [12], it is reasonable to modify the model to include this effect explicitly. Myers [14] has discussed explicit inclusion of nonideal effects in order to avoid the need for activity coefficients in adsorption on activated carbon. Thus, the steric factor may be looked upon as a lumped parameter which

includes a number of non-idealities of the mobile and stationary phase of which the dominant non-ideality is expected to be steric shielding.

Three major features of the SMA single-component isotherm should be noted. First, in dilute protein solutions, the partition ratio of each protein reduces to the following simple relationship:

$$\frac{Q_i}{C_i} = K_{1i}\left(\frac{\Lambda}{C_1}\right)^{\nu_i} \quad i = 2, \ldots, NC \tag{8}$$

Second, the maximum binding capacity of the stationary phase for a particular protein will be

$$Q_{i,\max} = \frac{\Lambda}{\nu_i + \sigma_i} \quad i = 2, \ldots, NC \tag{9}$$

Third, over the entire range of protein concentration, protein adsorption is enhanced by lowering the salt concentration in the mobile phase. These observations agree with experimental observations of the adsorption of both proteins and long-chain polyelectrolytes [15–18].

This model has previously been tested in a number of ways. SMA has been shown to represent single-component isotherms of proteins at varying salt concentrations [15] (see Appendix). The SMA formalism has been used in conjunction with an ideal model of chromatography to predict isotachic displacement chromatograms [16–18]. Further, it has been used in conjunction with a numerical model of chromatography to predict displacement development, confirming its ability to predict multi-component equilibrium [19]. The values of the SMA parameters employed in this study are shown in Table 1.

Table 1
Parameters employed in simulation

Solute	Characteristic charge (ν_i)	Equilibrium constant (K_{1i})	Steric factor (σ_i)
Sodium	1.00	1.00	0.0
Cytochrome *c*	6.15	$6.37 \cdot 10^{3}$	53.4

Column capacity (Λ) = 590 mM; void fraction (ε) = 0.70.

2.3. Field equations and boundary conditions

In ideal chromatography, transport within the chromatographic column is described by the following system of partial differential equations [20,21]:

$$\frac{\partial C_i}{\partial z} + \frac{\partial C_i}{\partial \tau} + \beta \frac{\partial Q_i}{\partial \tau} = 0 \quad i = 1, \ldots, NC \tag{10}$$

where β is a phase ratio, z is a non-dimensional measure of the axial position ($z = Z/L_{col}$) and τ is a dimensionless time unit ($\tau = t/t_0$). In these non-dimensional coordinates, the velocity of an unretained component in the mobile phase is unity. Non-dimensional time and distance units will be employed in the discussion that follows. Table 2 includes the actual experimental conditions in dimensional units.

In isocratic chromatography, the salt concentration is held constant at the column inlet:

$$C_1(\tau, 0) = C_{1,f} \tag{11}$$

where the subscript 1 refers to the counter ion. During operation, three sequential procedures are carried out on the column, equilibration, loading, and elution:

$$C_2(\tau < 0, 0) = 0 \qquad \text{(equilibration)} \tag{12a}$$

$$C_2(0 < \tau < \tau_f, 0) = C_{2,f} \qquad \text{(loading)} \tag{12b}$$

$$C_2(\tau > \tau_f, 0) = 0 \qquad \text{(elution)} \tag{12c}$$

where the subscript 2 refers to the protein and τ_f represents the duration of the feed pulse in dimensionless units.

The total concentration of components 1 and 2 (counter ion and protein) given in equivalents constitutes a third variable, C_T:

$$C_T(\tau < 0, 0) = C_{1,f} \tag{13a}$$

$$C_T(0 < \tau < \tau_f, 0) = C_{1,f} + \nu_2 C_{2,f} \tag{13b}$$

$$C_T(\tau > \tau_f, 0) = C_{1,f} \tag{13c}$$

Because adsorption of protein displaces a number of counter ions equivalent to the characteristic charge of the protein, ν_2, the disturbance of C_T due to the feed propagates through the column at the mobile phase velocity:

$$C_T(\tau, z) = C_T(\tau - z, 0) \tag{14}$$

Table 2
Non-linear elution cation-exchange chromatography: experimental conditions

Fig.	Feed volume (ml)	Flow-rate (ml/min)	Cytochrome *c* concentration (m*M*)	Sodium concentration (m*M*)
6	0.20	0.2	0.54	150
7	0.20	0.5	0.57	125
8	3.17	0.5	0.29	150

Mobile phase, sodium phosphate buffer (pH 6.0); column, 50 × 5 mm I.D.; column dead volume, 0.69 ml.

A plot of the behavior of C_T is shown in Fig. 2. Within zones 1, 2 and 3, C_T assumes the values $C_{1,f}$, $C_{1,f} + \nu_2 C_{2,f}$ and $C_{1,f}$, respectively. The line that separates zones 1 and 2 intersects the time axis at the moment that the feed pulse enters the inlet of the column. The line that separates zones 2 and 3 intersects the time axis at the moment the feed pulse ends ($\tau_f = 0.29$).

2.4. Solution of the model

The preceding field equations (Eq. 10), isotherm (Eqs. 5 and 7) and boundary conditions (Eqs. 11 and 12) may be solved to produce an ideal chromatogram. Rhee et al. [3] discussed a similar problem when equilibrium is governed by the Langmuir isotherm and only one component is present in the mobile phase. Realization that C_1 and C_2 are not independent (they are linked by C_T) and that the value of C_T at any point in the column is known through Eqs. 13 and 14 allows the approach of Rhee et al. to be applied to the solution of the problem at hand.

The behavior of the variable C_T has been presented in Fig. 2. The solution of the entire ideal model will be superimposed on this development graph. The goal of this process is to calculate the path of the shock that forms at the beginning of the protein peak and the pattern of the rarefaction wave that forms the tail. The shock is divided into three segments, which will be designated A, B and C. The solution will proceed in six steps as described below. On the basis of this description, this model may be implemented in a computer program or, more conveniently, in a computer spreadsheet.

Calculation of the initial frontal protein and salt concentrations

During injection of a feed pulse of finite width, the protein enters the column under conditions of frontal development. The mobile phase concentrations of protein ($C_{2,f}$) and salt ($C_{1,f}$) are the feed concentrations given in Eqs. 11 and 12. Solution of the isotherm, eqs. 5 and 7, allows the stationary phase concentrations of protein and salt to be calculated. As the mobile phase and stationary phase concentrations of protein and salt are uniform everywhere behind this front during the injection, this is called a zone of constant concentration, and the concentrations within the zone will be designated $C_{1,A}$, $C_{2,A}$, $Q_{1,A}$ and $Q_{2,A}$, where $C_{1,A} = C_{1,f}$ and $C_{2,A} = C_{2,f}$.

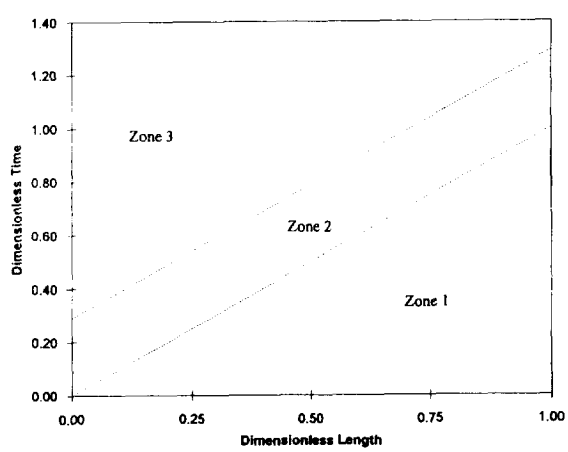

Fig. 2. Development of C_T for the case of isocratic protein elution. In zone 1, $C_T = C_{1,f}$, in zone 2, $C_T = C_{1,f} + \nu_2 C_{2,f}$; and in zone 3, $C_T = C_{1,f}$. For Figs. 2–4, elution of the protein cytochrome *c* in a mobile phase of 150 m*M* sodium at pH 6.0; the feed pulse was injected at a concentration of 0.54 m*M* over 0.29 dimensionless time units.

Calculation of shock segment A

The velocity of this initial front or "shock" may now be calculated. Because the zones in front of and behind the shock are zones of constant mobile and stationary phase concentration, the resulting shock moves along a straight line, given by the equation

$$\tau = \left(1 + \beta \cdot \frac{\Delta Q_{i,A}}{\Delta C_{i,A}}\right) z \quad i = 1 \text{ and } 2 \tag{15}$$

where $\Delta Q_{i,A}$ and $\Delta C_{i,B}$ represent the change in concentration across the shock. Because the protein concentration in front of the shock is zero, it is possible simply to write

$$\tau = \left(1 + \beta \cdot \frac{Q_{2,A}}{C_{2,A}}\right) z \tag{16}$$

where $C_{2,A}$ and $Q_{2,A}$ are the mobile and stationary phase concentrations of protein behind shock segment A.

Shock segment A originates at the point (0, 0) at which the feed is introduced into the column. Examining Fig. 3, it can be seen that the shock travels slower than the changes in total equivalents (C_T) which are plotted in both Figs. 2 and 3. The point at which the second change in total equivalents catches up with shock segment A is labeled K in Fig. 3. Point K is the end of shock segment A.

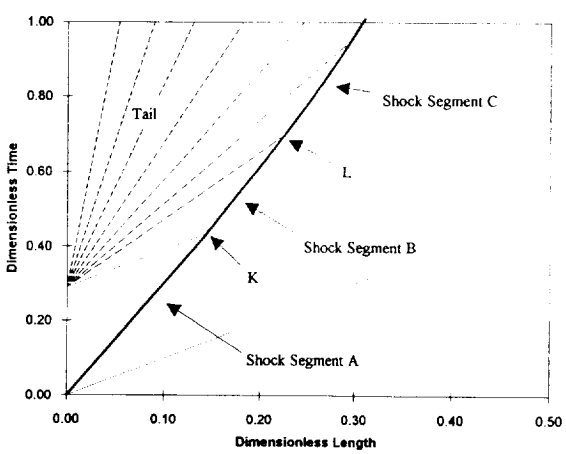

Fig. 3. Development plot for isocratic protein elution. Plot includes changes in the value of C_T (dotted lines), the protein front or "shock" (solid line) and characteristics of the tail or "rarefaction wave" (dashed lines). This figure represents an expanded view of one region of Fig. 4; the calculation was carried out with 50 characteristics in the rarefaction wave. Simulation conditions as in Fig. 2.

Calculation of second plateau concentration

On the basis of Eqs. 13 and 14, it can be seen that the second change in total ion concentration (C_T) passes through the column as a discontinuity traveling at the mobile phase velocity ($u_T = 1$). Of particular interest is the portion of the development plot (Fig. 3) from the end of the feed pulse at $\tau = 0.29$ to the point designated K. Along this dotted line, the change in C_T is made up of changes in the mobile phase concentrations of protein (C_2) and salt (C_1). Below this dotted line, the mobile and stationary phase concentrations have already been calculated. Above this dotted line, they are unknown.

Since the values of C_1 and C_2 change across this line, the line represents a discontinuity in the value of both these quantities. The velocity of any discontinuity within the column is given by the expression

$$u_{sh} = \frac{1}{1 + \beta \cdot \dfrac{\Delta Q_i}{\Delta C_i}} \quad i = 1 \text{ and } 2 \tag{17}$$

As this discontinuity moves through the column with a velocity of unity ($u_{sh} = u_T = 1$), it can be seen that $\Delta Q_i / \Delta C_i = 0$. Hence the bound concentrations of protein and salt do not change across the discontinuity caused by the change in C_T, and are know to be $Q_{2,B} = Q_{2,A}$ and $Q_{1,B} = Q_{1,A}$. However, the mobile phase concentrations do change and must be calculated. Since the total ion concentration above the dotted line (after the discontinuity) is known ($C_T = C_{1,f}$) and since $Q_{2,B}$ and $Q_{1,B}$ have already been established, the individual mobile phase concentrations $C_{1,B}$ and $C_{2,B}$ may be calculated using the SMA isotherm (Eqs. 5 and 7).

It should be noted that, if one attempted to describe the protein's equilibrium using the Langmuir isotherm, such a two-plateau solution would not exist. However, when the SMA for-

malism is employed, the existence of two plateaus in the simulation of the development of a pulse of finite width is a necessity. Experimental results that include such two-plateau development will be presented below.

Calculation of the tail

In order to calculate the boundaries of this second region of constant concentration on the development plot, it is necessary to examine the rarefaction wave or tail of the protein band. The tail exists entirely within zone 3 of Fig. 2, where the total concentration of protein and salt given in equivalents is known ($C_T = C_{1,f}$).

The behavior of the tail may be calculated using the method of characteristics. An infinite number of "characteristics" (lines of constant protein and salt concentration) fan out from the end of the feed pulse at the point (τ_f, 0). The equation of the characteristics is

$$\tau = \tau_f + \left(1 + \beta \cdot \frac{\partial Q_2}{\partial C_2}\right) z \tag{18}$$

where the partial derivative $\partial Q_2/\partial C_2$ is evaluated over the range $0 \leq C_2 \leq C_{2,B}$. Because C_1 and C_2 remain constant along any characteristic, the partial derivative $\partial Q_2/\partial C_2$ remains constant along that characteristic, and the resulting characteristic is a straight line.

In the limiting case of $C_2 = 0$ (i.e., the case of infinite dilution with respect to protein), the partial derivative will be given by

$$\frac{\partial Q_2}{\partial C_2} = K_{12}\left(\frac{\Lambda}{C_T}\right)^{\nu_2} \tag{19}$$

Use of Eq. 19 in the characteristic equation will result in calculation of the slowest characteristic within the tail. The point at which this characteristic reaches the end of the column is labeled M in Fig. 4.

For higher concentrations of protein, the expression for the differential is more complex. Recalling that C_T is constant and known through Eq. 13c and that Eq. 7 describes the stationary phase capacity, differentiation of Eq. 5 leads to the expression

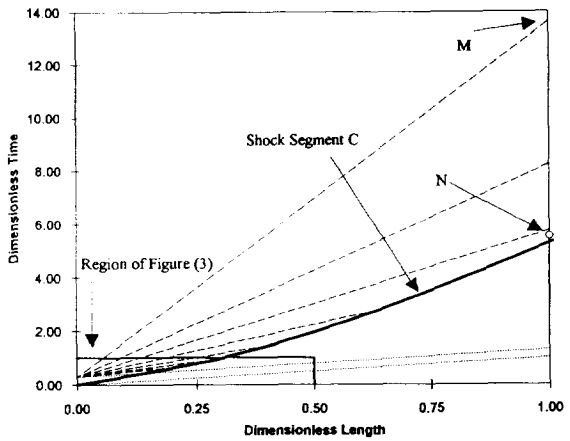

Fig. 4. Development plot for isocratic protein elution. Plot includes changes in the value of C_T (dotted lines), the protein front or "shock" (solid line), characteristics of the tail or "rarefaction wave" (dashed lines) and the estimate of the breakthrough obtained by quadrature applied to Eq. 30 (open circle). The calculation was carried out with 50 characteristics in the rarefaction wave. Simulation conditions as in Fig. 2.

$$\frac{\partial Q_2}{\partial C_2} = \frac{\dfrac{Q_2}{C_2} + \nu_2^2 \cdot \dfrac{Q_2}{C_1}}{1 - \nu_2 + \nu_2 \cdot \dfrac{\Lambda}{\bar{Q}_1}} \tag{20}$$

which is valid throughout the tail and which simplifies to Eq. 19 under conditions of infinite dilution with respect to the protein. Given an arbitrary value of C_2 and using the isotherm in conjunction with the known value of C_T, the quantities C_1, Q_2 and $\bar{Q}_1$ may be calculated. Subsequently, the corresponding characteristic may be calculated using Eqs. 18 and 20. Discretization of C_2 over the range $0 \leq C_2 \leq C_{2,B}$ leads to a fan of the type depicted by the dashed lines in Fig. 4. Below, these characteristics will be used to generate simulated chromatograms.

However, discretization over C_2 is not the method of choice. Because Q_2 and $\bar{Q}_1$ are implicit functions of C_2 and C_1, discretization over C_2 requires a numerical calculation using a Newton–Raphson method for each characteristic. In contrast, when C_T is known, C_2, C_1, Q_2 and $\bar{Q}_1$ are explicit functions of $\bar{Q}_1/C_1$. Thus, the appropriate discretization is obtained using

the variable $\bar{Q}_1/C_1$ over the range $\Lambda/C_T \leq \bar{Q}_1/C_1 \leq \bar{Q}_{1,B}/C_{1,B}$. No matter how many characteristics are employed, the resulting method for generating chromatograms requires only two applications of a Newton–Raphson method.

It should be noted that the ratio $\bar{Q}_1/C_1$ constitutes a fundamental variable of non-linear chromatography when equilibrium is described by the SMA formalism. The separation factor under concentrated conditions is given by the expression

$$\alpha_{ij} = \frac{Q_i}{C_i} \cdot \frac{C_i}{Q_j} = \left(\frac{K_{1j}}{K_{1j}}\right)\left(\frac{\bar{Q}_1}{C_1}\right)^{(\nu_i - \nu_j)} \tag{21}$$

For displacement chromatography, using the dynamic affinity theory of Brooks and Cramer, [22], the affinity parameter λ_i is defined by the following expression:

$$\lambda_i = \left(\frac{K_{1i}}{\Delta}\right)^{1/\nu_i} = \left(\frac{C_1}{\bar{Q}_1}\right)_i \tag{22}$$

where Δ is the partition coefficient of the displacer (Q_d/C_d) and $(\bar{Q}_1/C_1)_i$ is the ratio $\bar{Q}_1/C_1$ defined by the protein microenvironment. It is no coincidence that the ratio $\bar{Q}_1/C_1$ appears in the separation factor and is related to the affinity parameter. In fact, the ratio of the sites on the ion-exchange surface available for exchange to the mobile phase salt concentration is a fundamental variable of nonlinear ion-exchange chromatography. Rearrangement of Eq. 5 make it clear that this ratio

$$Q_i = K_{1i}\left(\frac{\bar{Q}_1}{C_1}\right)^{\nu_i} C_i \quad i = 2, \ldots, NC \tag{23}$$

is directly related to the partition coefficient under linear and non-linear, single-component and multi-component conditions.

Calculation of the development boundaries of the second plateau

Having calculated the concentrations of protein and salt present in the mobile and stationary phases immediately after the second C_T discontinuity, what are the boundaries of this region in the development plot? One boundary will be the characteristic of the tail (rarefaction wave) calculated by solving Eqs. 18 and 20 for the value $C_{2,B}$ (i.e. the value $\bar{Q}_{1,B}/C_{1,B}$). This characteristic is depicted in Fig. 3 as the dashed line with the shallowest slope (highest velocity).

The second boundary of this constant concentration zone will begin at the point labeled K on the development plot Fig. 3. At this point, shock segment A ends and shock segment B begins. Shock segment B represents the path of a front of constant concentration and follows the straight line given by

$$\tau = \left(1 + \beta \cdot \frac{Q_{2,B}}{C_{2,B}}\right) z \tag{24}$$

Having calculated the two previously unknown boundaries of the second zone of constant concentration, the intersection of these two boundaries may also be calculated. This is the point at which the rarefaction wave (tail) reaches the front of the protein pulse, and it is the end of shock segment B. This point is labeled L in Fig. 3.

Calculation of shock segment C

After the rarefaction wave has reached the front of the protein pulse, the concentration of protein on the left side of the shock begins to decline. As a result, the last segment of the shock is not a straight line and a process of integration will be required in order to establish this segment of the shock path. In the discussion of the development of a peak of finite width by Rhee et al. [3], the Langmuir isotherm was employed. As a result, the integration could be carried out analytically. Because the SMA formalism has a more complex form than the Langmuir isotherm, no simple analytical method could be developed. However, two separate methods of numerical integration will be presented below. The first method calculates the path of the shock through the region of curvature and the second determines the breakthrough of the protein front without calculating the shock path. The second method serves as an independent check of the accuracy of the first method.

The goal of this calculation is to extend the shock path from the point L in Fig. 3 to the coordinate $z = 1$ (when the shock emerges from the column). Examination of Figs. 3 and 4 reveals that the characteristics of the tail meet the protein shock after point L in the region of curvature. The velocity of the shock along each characteristic is known exactly and is given by the following version of Eq. 17:

$$u_{sh} = \frac{1}{1 + \beta \cdot \frac{Q_2}{C_2}} \tag{25}$$

The velocity of the characteristics themselves may also be calculated. Consideration of Eq. 18 gives the velocity of any characteristic:

$$u_{char} = \frac{1}{1 + \beta \cdot \frac{\partial Q_2}{\partial C_2}} \tag{26}$$

where the partial derivative can be calculated using Eq. 20. Since the velocity of the characteristics (u_{char}) and the velocity of the shock along each characteristic (u_{sh}) are both known exactly, a numerical technique may be developed to calculate the path of the shock.

The numerical integration begins at point L in Fig. 3. This point corresponds to the intersection of the protein shock and the fastest characteristic of the tail and will be designated (τ_0, z_0). To calculate each new point (τ_{i+1}, z_{i+1}) along the protein shock, the velocity of the shock will be estimated to be the velocity at the current point ($u_{sh,i}$). The intersection of this linear approximation of the shock and the next characteristic (numbered $i + 1$) will then be calculated. The non-dimensional coordinates of this intersection are

$$z_{i+1} = \frac{\tau_f - \tau_i + \frac{z_i}{u_{sh,i}}}{\frac{1}{u_{sh,i}} - \frac{1}{u_{char,i+1}}} \tag{27}$$

$$\tau_{i+1} = \frac{z_{i+1}}{u_{char,i+1}} + \tau_f \tag{28}$$

The results of such a numerical integration are shown in Fig. 4. For clarity, only a fraction of the characteristics employed in the integration are shown in Fig. 4. As the number of characteristics employed in the calculation is increased, the numerical approximation of the shock path will converge to the actual path (the rate of convergence is discussed below). Having calculated the shock path and the rarefaction wave, it is possible to generate simulated chromatograms.

Before these simulated chromatograms are presented, a second independent method to calculate of the breakthrough time of the protein band, but not the shock path, will be presented. The mass of protein injected into the column may be calculated:

$$M_{inj} = C_{2,f} \tau_f V_0 \tag{29}$$

where V_0 is the dead volume of the column. Within the ideal theory of chromatography, a peak resulting from an injection of arbitrary concentration ($C_{2,f}$) and width (τ_f) will always finish eluting from the column at a time dictated by the protein's velocity at infinite dilution and the width of the injection volume. This point (τ_{id}, 1) is labeled M in Fig. 4. If an integration of the mass eluting from the column is carried out, it is expected that the following equation will be satisfied:

$$M_{inj} = V_0 \int_{\tau_{bt}}^{\tau_{id}} C_2(\tau, 1)\, d\tau = -V_0 \int_{\tau_{id}}^{\tau_{bt}} C_2(\tau, 1)\, d\tau \tag{30}$$

where $C_2(\tau, 1)$ is the concentration of protein eluting from the end of the column at non-dimensional time τ and τ_{bt} and τ_{id} are the non-dimensional times at which the protein peak breaks through at the end of the column and at which the protein peak finishes eluting from the column, respectively.

The integral Eq. 30 may be evaluated numerically for the purpose of calculating τ_{bt}. By starting at the tail of the protein band at $\tau = \tau_{id}$ and $C_2 = 0$, it is possible to integrate backwards in time using a method of quadrature such as the trapezoid rule. The process of summation which approximates the integral Eq. 30 will continue as

long as the summation is less than the actual mass injected given by Eq. 29.

If a method of quadrature that overestimates the area within the tail of the chromatogram is employed (e.g., the trapezoid rule), the resulting estimate of τ_{bt} will be slightly later than the true value. In contrast, the numerical method for estimating the shock path described by Eqs. 27 and 28 will result in estimates of τ_{bt} that are slightly early. Thus, if the estimates of τ_{bt} obtained by the two methods agree within a prespecified tolerance, the accuracy of the shock path calculation can be considered confirmed.

The point (τ_{bt}, 1) estimated by quadrature applied to Eq. 30 is represented by an open circle labeled N in Fig. 4. Comparison of the arrival time of the shock with this open circle reveals a small disagreement of the two methods for a calculation using 50 characteristics. By increasing the number of characteristics employed in the calculation, an arbitrary degree of accuracy may be obtained.

Table 3 presents data on the convergence of the numerical integration scheme of Eqs. 27 and 28. The first column of the table presents the number of characteristics employed in calculation of τ_{bt}. The second column presents the value of τ_{bt} obtained by numerical integration along the shock path using Eqs. 27 and 28. The third column presents the change in τ_{bt} with each increase in the number of characteristics employed. Examination of the third column reveals that the numerical scheme converges linearly with the number of characteristics employed. By extrapolating this linear trend to an infinite number of characteristics, it is possible to estimate the true value of τ_{bt}. The result of that extrapolation is contained within the bottom row of the table. The final column of the table presents the percentage error of each of the estimates with respect to the extrapolated value of τ_{bt}.

Table 3
Convergence of numerical approximation of shock segment C

No. of characteristics	τ_{bt} (method 1)	$\Delta\tau_{bt}$	Error (%)
25	5.155		−4.9
50	5.283	0.128	−2.5
100	5.351	0.068	−1.2
200	5.384	0.033	−0.6
400	5.401	0.017	−0.3
∞[a]	5.418	0.017	0.0

[a] The value of τ_{bt} for an infinite number of characteristics was calculated by extrapolation.

During the process of integrating Eq. 30, if the edge of a trapezoid closely coincides with the true value of τ_{bt}, an extremely accurate estimate of τ_{bt} will be obtained. Thus, the values of $\Delta\tau_{bt}$ would not be expected to converge smoothly in the second method. However, its maximum possible error would be bounded and is expected to converge in a manner similar to the first method.

Because only two Newton–Raphson calculations are required in order to solve the model, a calculation involving 400 characteristics is only slightly slower than one involving 25. All calculations were carried out using the Microsoft Excel program on a computer equipped with an Intel 80486 CPU, and the longest required less than 5 s.

Three types of chromatograms that may result

Three broad categories of chromatograms may result from the preceding calculation. If the peak elutes from the column after the points K and L in Fig. 3 have been reached within the column, a non-linear peak without any regions of constant concentration will emerge from the column. Such a peak is shown in Fig. 5a. If point K has been reached inside the column but not point L, then a peak with a single plateau will emerge from the column (Fig. 5b). If neither point K nor point L is reached inside the column, a peak with a double plateau will emerge from the column (Fig. 5c). Assuming that all the operating conditions have been held constant except feed volume, Fig. 5b represents a larger feed volume than Fig. 5a, and Fig. 5c represents a larger feed volume than Fig. 5b.

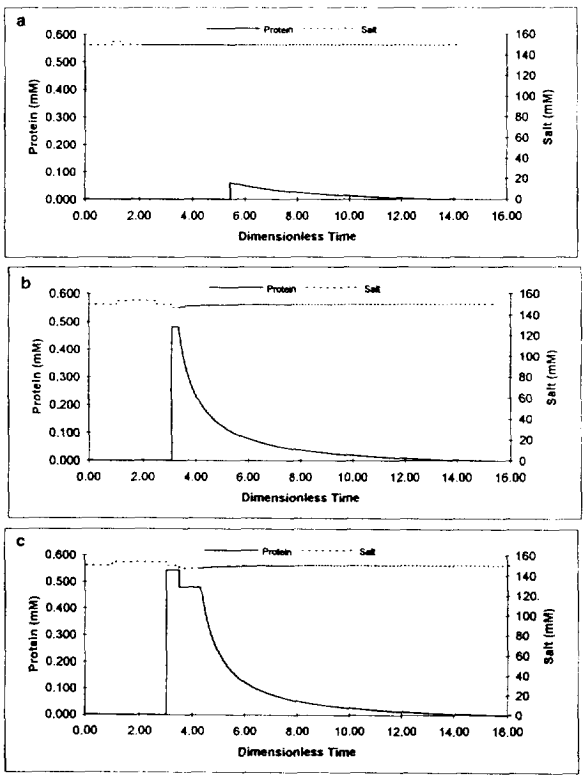

Fig. 5. The three categories of non-linear peaks observed in simulated chromatograms. (a) Feed volume of 0.29 dimensionless time units; simulation conditions as in Fig. 2. (b) Feed volume increased to 1.5 dimensionless time units. (c) Feed volume increased to 2.5 dimensionless time units. The calculations were carried out with 400 characteristics in the rarefaction wave.

3. Experimental

3.1. Materials

Sodium monobasic phosphate, sodium dibasic phosphate, and cytochrome *c* were purchased from Sigma (St. Louis, MO, USA). Sodium chloride was purchased from Aldrich (Milwaukee, WI, USA). Orthophosphoric acid was purchased from Fisher (Rochester, NY, USA). The strong cation-exchange column employed (sulfopropyl, 8 μm, 50 × 5 mm I.D.) was a gift from Waters Chromatography Division of Millipore (Milford, MA, USA).

The carrier was buffered using a solution of sodium monobasic phosphate and sodium dibasic phosphate, the ratio being chosen to give the appropriate pH range. The desired concentration of sodium ions was obtained subsequently by addition of sodium chloride. Finally, the pH was adjusted using phosphoric acid.

3.2. Apparatus

The chromatograph consisted of an LC 2150 pump (Pharmacia–LKB Biotechnology, Piscataway, NJ, USA) connected to the column via a C10W ten-port injector (Valco, Houston, TX, USA). The column effluent was monitored using a Model 757 Spectroflow UV–Vis detector (Applied Biosystems, Ramsey, NJ, USA). The detector signal was recorded using a Powermate 2 personal computer (NEC, Tokyo, Japan) which was running Maxima 820 data collection software (Waters Chromatography Division, Millipore). Data generated in this study were exported to the Microsoft Excel spreadsheet program for analysis.

3.3. Parameter estimation

The estimation of the SMA equilibrium parameters which appear in Table 1 has been discussed in detail previously [15]. In order to determine the column capacity Λ, the column was equilibrated with a carrier of 100 m*M* sodium (pH 6.0). Subsequently, a front of 1 *M* ammonium sulfate was passed through the column, and the column effluent was collected for analysis. The bed capacity was determined by measuring the amount of sodium displaced by the ammonium front.

In order to estimate the characteristic charge ν_i and equilibrium constant K_{1i} of the protein, linear elution experiments were conducted at various mobile phase salt concentrations. The resulting data was fitted to the linearized form of Eq. 1:

$$\log (k_i') = \log (\beta K_{1i} \Lambda^{\nu_i}) - \nu_i \log C_1 \qquad (31)$$

This fitting procedure resulted in an estimate of the characteristic charge ν_i of 6.15 with an uncertainty of ±0.25 and an estimate of the intercept log $(\beta K_{1,i}\Lambda^{\nu_i})$ of 14.46 with an uncertainty of ±0.57 (95% confidence interval based on the Student t-distribution).

The concentration of protein bound in frontal operation $(Q_{2,f})$ may be determined using the expression

$$Q_{2,\mathrm{exp}} = \left(\frac{V_B}{V_0} - 1\right) \cdot \frac{C_{2,f}}{\beta} \tag{32}$$

where $C_{2,f}$ is the protein concentration of the front, V_B is the breakthrough volume of the front, V_0 is the dead volume of the column and β is the phase ratio. Using Eq. 32, pairs of known values of $C_{2,f}$ and $Q_{2,f}$ may be established in order to represent the single component isotherm at various salt concentrations.

Having established the isotherm experimentally, an estimate of the steric factor σ_i may now be obtained. Only a single point in the non-linear region of the isotherm, represented by a pair of values of $C_{2,f}$ and $Q_{2,f}$, is required. Of course, the protein concentration $C_{2,f}$ should be relatively high in order to insure that the non-linear region of the isotherm has been reached. Greater accuracy can be expected by conducting frontal experiments at more than one protein concentration and at more than one salt concentration.

Because SMA is an implicit isotherm, calculation of the concentration of bound protein $(Q_{2,\mathrm{SMA}})$ on the basis of known values of mobile phase protein and salt concentrations ($C_{2,f}$ and $C_{1,f}$) requires use of a Newton–Raphson technique. (The designation SMA after $Q_{2,\mathrm{SMA}}$ indicates that this is an estimate made by the SMA formalism.) However, the mobile phase concentration of protein $(C_{2,\mathrm{SMA}})$ may be calculated analytically based on known values of mobile phase salt concentration and stationary phase protein concentration (C_{1f} and $Q_{2,f}$):

$$C_{2,\mathrm{SMA}} = \left[\frac{C_{1,f}}{\Lambda - (\nu_2 + \sigma_2)Q_{2,f}}\right]^{\nu_i} \frac{Q_{2,f}}{K_{12}} \tag{33}$$

Eq. 33 may be used in conjunction with the experimental protein isotherm in order to estimate the steric factor σ_i. The residuals between the experimental protein concentration $(C_{2,f})$ used in Eq. 32 and the estimate of the protein concentration $(C_{2,\mathrm{SMA}})$ obtained from Eq. 33 may be calculated as a function of the steric factor. Minimization of the sum of squares of the residuals using a Newton–Raphson technique will establish the estimated steric factor.

The use of Eq. 33 will be designated the "frontal method" of determination of the steric factor. In this work, multiple non-linear frontal experiments were employed to estimate a steric factor of 53.4. These points are shown in conjunction with the corresponding SMA isotherms in the Appendix.

3.4. Conversion of detector response

In order to compare the predictions obtained from the ideal model presented above with chromatographic experiments, non-linear elution experiments were conducted at 150 and 125 mM salt concentrations. The chromatograms were collected using Maxima 820 data collection software and saved for later analysis. The original data were obtained in units of μV (detector response) versus minutes. During data reduction, the time axis was converted into dimensionless time units. (An unretained tracer capable of exploring all of the pores would emerge from the column at one dimensionless time unit. No measurable pore exclusion of cytochrome c was observed). The detector response was converted from μV to mM cytochrome c using appropriate conversion factors obtained from linear plots of concentration versus detector response.

4. Results and discussion

Having presented the theoretical model of isocratic elution of a pulse of finite width and height, the focus of the discussion will be on a small number of carefully selected experiments to document both the ability of the model to predict this phenomenon and the limitations of the model. Two relatively important constraints

on the model should be understood at the outset. First, ideal chromatography ignores the effect of Taylor dispersion during convective transport within the column and the effects of finite rates of mass transport across the film surrounding the stationary phase particles and within the pores of the particles [1]. As a result, the predictions of an ideal model do not have the rounded contours of experimental chromatograms. Nevertheless, under non-linear conditions, it is expected that an ideal model will provide reasonable predictions of experimental results since thermodynamic spreading of the tail predominates over mass transfer effects. Second, this model only attempts to account for the elution of a single protein. In order to model multi-component separations, interaction of multiple shocks and rarefaction waves must be considered. Typically, such problems are solved by resort to numerical techniques such as finite difference or finite element methods.

Fig. 6 shows the non-linear elution of cytochrome *c* at 150 m*M* salt. As can be seen, the infinite dilution retention of the protein is well predicted at 13.6 dimensionless time units. Slight experimental tailing beyond this point is attributable to the dispersion observed in the column which is not included in the ideal model. The degree of tailing observed in the experimental chromatogram is well matched by the simulation. The front of the experimental cytochrome *c* band is more disperse, but examination of the breakthrough time of the front measured at half-height yields a value of τ_{bt} almost identical with the simulated value (5.4 dimensionless time units).

Fig. 7 shows the non-linear elution of cytochrome *c* at 125 m*M* salt. The decrease in salt concentration has sharply increased the retention of the protein. The infinite dilution retention of the protein is now in the neighborhood of 39 dimensionless time units. And, the maximum concentration of the experimental chromatogram has decreased to approximately 0.015 m*M*. Again, the experimentally observed tailing is well simulated by this model.

Recalling the discussion of Figs. 3 and 4, all peaks go through a period of development in which they are characterized by two plateaus (as depicted in Fig. 5c). Subsequently, the chromatographic band may develop into a band of one plateau (Fig. 5b) or no plateaus (Fig. 5a) if the column is long enough. Having observed two highly tailed peaks of the type depicted in Fig. 5a, it is worth examining the earlier development of a peak of finite width. For this purpose, the feed pulse was increased to a width of 4.6 dimensionless time units and a concentration of 0.29 m*M* cytochrome *c*. Fig. 8 depicts the re-

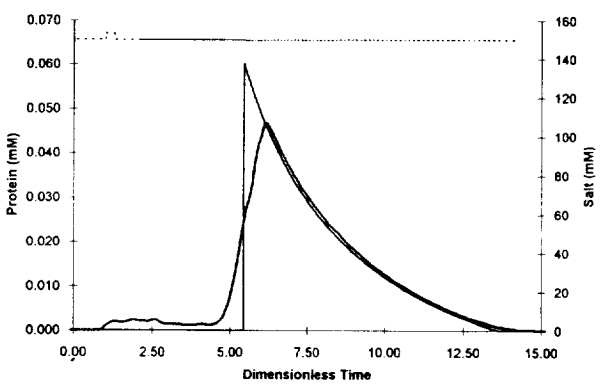

Fig. 6. Elution chromatogram (thick solid line) and simulation (thin solid line) of the protein cytochrome *c* in a mobile phase of 150 m*M* sodium at pH 6.0. The simulated salt profile is depicted as a dotted line. The feed pulse was injected at a concentration of 0.54 m*M* over 0.29 dimensionless time units. The calculation was carried out with 400 characteristics in the rarefaction wave.

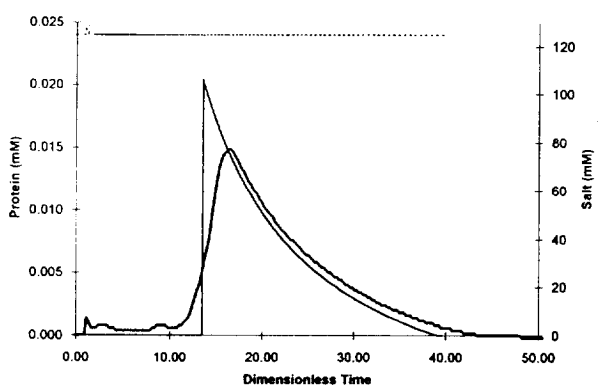

Fig. 7. Elution chromatogram (thick solid line) and simulation (thin solid line) of the protein cytochrome *c* in a mobile phase of 125 m*M* sodium at pH 6.0. The simulated salt profile is depicted as a dotted line. The feed pulse was injected at a concentration of 0.57 m*M* over 0.29 dimensionless time units. The calculation was carried out with 400 characteristics in the rarefaction wave.

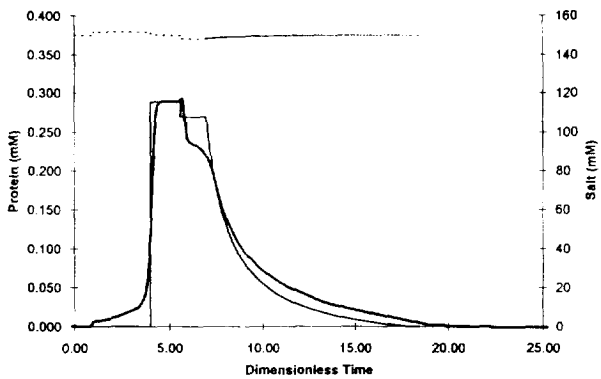

Fig. 8. Elution chromatogram (thick solid line) and simulation (thin solid line) of the protein cytochrome *c* in a mobile phase of 150 m*M* sodium at pH 6.0. The simulated salt profile is depicted as a dotted line. The feed pulse was injected at a concentration of 0.29 m*M* over 4.6 dimensionless time units. The calculation was carried out with 400 characteristics in the rarefaction wave.

sulting two-plateau protein band. The infinite dilution retention is correctly predicted at 17.9 dimensionless time units. (Slight dispersion is observed past that point.) The tail is characterized by the correct degree of tailing. Before the tail, two regions of constant concentration are observed. Remarkable points about these two plateaus are that (1) to the authors' knowledge, no similar peak shape has been reported for isocratic chromatography and (2) no existing model of protein adsorption, other than SMA, would allow this result to be understood. While there is a slight disagreement in the exact concentration (0.23 m*M* experimental compared with 0.27 m*M* simulated), this result nevertheless demonstrates that SMA is uniquely well suited to describe the equilibrium in non-linear ion-exchange chromatography. (See the Appendix for a further discussion of the representation of protein isotherms in ion-exchange chromatography.)

Also included in Figs. 6–8 are the predicted salt concentrations of the model Examination of these salt profiles reveals that the salt concentration changes in isocratic chromatography are small. In Fig. 6, a pulse increase of salt is observed at 1 dimensionless time unit; this pulse was caused by injection of cytochrome *c* during the feed cycle. Subsequently, a slight decrease in salt occurs at the time that the protein peak elutes; this decrease allows C_T to remain constant, satisfying Eqs. 13 and 14. In Fig. 8, the effect of varying C_T and the effect of the elution of the protein peak depressing the salt concentration interact with each other. In fact, these effects are so subtle that most analyses would ignore them completely. However, they must be included if the two-plateau shape of Fig. 8 is to be understood.

Reflection on these simulated salt profiles reveals why the model did not predict more precisely the concentration of the second plateau. In Fig. 8, the carrier sodium concentration is 150 m*M*, the maximum deviation in the simulated salt profile is 151.18 m*M* and the minimum is 148.3 m*M*. Since these changes in salt concentration have such small magnitude, it is relatively easy for the various transport non-idealities to smooth out these changes, leading to a less pronounced two-plateau pattern. However, without the understanding offered by this model, it is likely that observation of such a double plateau would lead to the unwarranted conclusion that the product was not pure.

In Fig. 9, four non-linear peaks are shown. The bold solid line is the experimental peak already seen in Fig. 6. The lighter solid line is

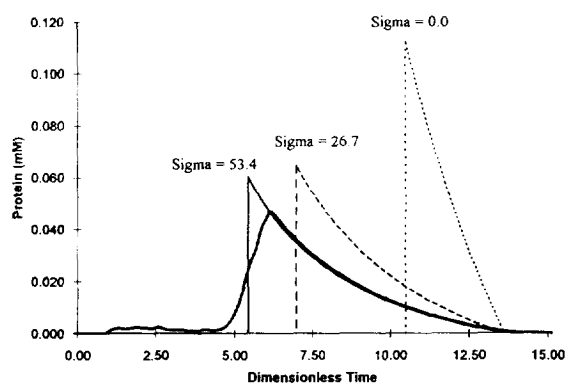

Fig. 9. Elution chromatogram (thick solid line) of the protein cytochrome *c* in a mobile phase of 150 m*M* sodium at pH 6.0. The feed pulse was injected at a concentration of 0.54 m*M* in 0.29 column volumes. Simulations were conducted for these conditions using a steric factor σ_2 of 53.4 (thin solid line), 26.7 (dashed line) and 0.0 (dotted line). The calculations were carried out with 400 characteristics in the rarefaction wave.

the model prediction shown in Fig. 6 for which the steric factor σ_2 is 53.4 (estimated using the frontal method). The dashed line utilizes the same simulation conditions as the solid line except that the steric factor is 26.7, half of the correct value. The dotted line was simulated using a steric factor of 0.0. Examination of Fig. 9 reveals clearly that use of a steric factor of 0.0 will result in significantly incorrect predictions of the non-linear band shape. A number of recent models of ion-exchange equilibrium fail to account for steric effects [8,9]. It is expected that chromatographic models based on such equilibrium will have difficulty accounting for non-linear adsorption. Examination of the peaks generated using steric factors of 53.4 and 26.7 leads to a preference for the 53.4 value. In particular, the tailing is modeled substantially better by the larger σ_2 value, and the breakthrough is estimated more accurately.

Having shown that the model can predict the elution of proteins and that the proper selection of the steric factor is important to accurate modeling of non-linear elution, a method of estimating the steric factor using a non-linear peak will now be discussed. A number of workers have discussed the use of chromatographic models in estimating Langmuir isotherm parameters [23,24]. Although the SMA model is different from the Langmuir isotherm, certain similarities exist between this earlier work and the technique presented below. In particular, the goal of all these methods is to decrease the number of frontal experiments required in parameter estimation, saving time and protein. Also, they take advantage of the fact that, in non-linear chromatography, the solute velocity depends on the mobile phase concentration of the solute.

The "non-linear peak method" of estimating the steric factor of a protein operates by minimizing the residuals between the experimental peak and the simulated chromatogram. Examination of Fig. 9 suggests that focusing on the residuals calculated in the tail (rather than residuals taken in the neighborhood of the breakthrough) would be the most effective strategy. In order to test this method of σ_2 estimation, twelve data points (concentration–elution time pairs) were selected from the experimental chromatogram depicted in Fig. 9. These points were equally spaced between 7.1 and 12.4 dimensionless time units. Using Eqs. 18 and 20, the characteristics corresponding to the selected concentrations were calculated. The residuals between the experimental elution times of these concentrations and the times dictated by the characteristics were then calculated. The value of σ_2 which minimized the sum of squares of the residuals was 50.3. From this calculation, it can be seen that reasonable estimates of the steric factor σ_2 may be obtained by this method.

5. Conclusions

The traditional view of adsorption based on the Langmuir isotherm is inadequate for many of the chromatographic systems employed today. In particular, methods development in the preparative ion-exchange chromatography of proteins demand a rigorous yet convenient description of the salt dependence of binding and of non-linear adsorption. The steric mass action (SMA) model of ion exchange offers such a formalism.

Whether used in a simple, ideal model as presented here or in conjunction with an elaborate multi-component numerical model, the SMA formalism offers the ability to predict elution at various salt concentrations and also non-linear absorption and displacement effects. Because the SMA model builds on existing work that originated with the seminal paper by Boardman and Partridge [5], its use should be easily understood by both academics and process development professionals.

As another step in the adoption of such a model to process development, this paper has focused on two important effects in preparative chromatography: the salt dependence of protein binding and non-linear adsorption. The model that was presented can be easily implemented using one of the spreadsheets widely available for the personal computer. Having such a model available during parameter estimation or process

design can assist the separation scientist in methods development and optimization.

Acknowledgements

The authors acknowledge Millipore for providing the data collection system and the stationary phase employed. This research was supported by a Presidential Young Investigator Award to S.M.C. from the National Science Foundation.

Symbols

C	mobile phase concentration (mM)
$C_{i,\mathrm{A}}$	mobile phase concentration behind shock segment A (mM)
$C_{i,\mathrm{B}}$	mobile phase concentration behind shock segment B (mM)
$C_{i,\mathrm{f}}$	feed concentration at column inlet (mM)
F_i	function which returns Q_i when given $C_1, \ldots, C_{NC}$ (mM)
K_{1i}	equilibrium constant
k'	capacity factor
K	point of transition from shock segment A to shock segment B
L	point of transition from shock segment B to shock segment C
L_{col}	column length (cm)
M	point at which the tail of the chromatographic band elutes from the column
M_{inj}	mass of protein injected (μmol)
NC	number of components present in mobile phase
Q_i	stationary phase concentration (mM)
$Q_{i,\mathrm{A}}$	stationary phase concentration behind shock segment A (mM)
$Q_{i,\mathrm{B}}$	stationary phase concentration behind shock segment B (mM)
$Q_{i,\max}$	maximum possible single-component bound protein concentration (mM)
$\bar{Q}_1$	bound salt which is not sterically shielded (mM)
$\hat{Q}_1$	bound salt which is sterically shielded (mM)
$\bar{Q}_{1,\mathrm{B}}/C_{1,\mathrm{B}}$	ratio $\bar{Q}_1/C_1$ in constant concentration zone behind shock segment B
t	time dimension (s)
u_{char}	characteristic velocity (cm/s)
u_{sh}	shock velocity (cm/s)
u_0	chromatographic velocity, $u_0 = u_s/\varepsilon$ (cm/s)
V_0	dead volume of the column determined by a small tracer molecule (ml)
Z	axial position in column (cm)
z	dimensional axial position (Z/L)
z_i	ith position in the numerical integration of shock segment C

Greek letters

β	phase ratio $[(1-\varepsilon)/\varepsilon]$
Δ	change in a variable across a discontinuity
ε	void fraction
Λ	column capacity (mM)
ν_i	characteristic charge
σ_i	steric factor
τ	dimensionless time or column dead volumes ($\tau = t/t_0 = V/V_0$)
τ_{f}	dimensionless feed pulse time
τ_i	ith time in the numerical integration of shocked segment C

Subscripts

i	mobile/stationary phase component number ($i = 1$ designates salt)

Appendix

An important goal of this paper is to suggest that the SMA formalism is a superior method of depicting ion-exchange adsorption of proteins in chromatography. While the main body of this paper focuses on chromatographic development in nonlinear chromatography, this Appendix will be devoted to the depiction of isotherms. The parameter estimation process was described briefly in the main body of this paper. Within this Appendix, three isotherms will be compared for their efficacy at depicting protein adsorption

data. The first is the SMA formalism [13]. The second is the SDM/electroneutrality model [8,9]. The third formalism is the modifier-dependent Langmuir isotherm of Antia and Horváth [25]:

$$Q_i = \frac{a_i C_s^{-Z} C_i}{1 + \sum_{j=1}^{NC} \frac{a_j}{\lambda_j} C_s^{-Z} C_j} \quad \text{(A1)}$$

where C_s is the mobile phase salt concentration, C_i and Q_i are the mobile phase and stationary phase protein concentrations and Z_i, a_i and λ_i are parameters of the model. The modifier-dependent Langmuir was not employed in the main text because it would have been incapable of predicting the two-plateau peak shape.

In parameter estimation, the most reasonable approach in fitting a three-parameter model to experimental data is to use two parameters to fit the region of infinite dilution and to use the third parameter to fit the non-linear region of the isotherm. That is the approach described in the section of this paper devoted to parameter estimation for the SMA formalism. The benefit of this method is that, is that, by devoting two parameters to the infinite dilution data, chromatograms simulated at low concentrations should be fairly accurate. Any deviations between the model and the experiment will appear in the high-concentration regime.

Adopting this philosophy of fitting, all three of the models mentioned above should be able to predict low concentration [log(k') versus log(salt concentration) data] well. The data set employed to test the non-linear predictive capacity of these models consisted of cytochrome c data taken using frontal chromatography at 90, 125 and 150 mM sodium. The SMA formalism treated these data with little difficulty, as seen in Fig. A1a. The steric factor employed to obtain this fit was 53.4.

The SDM/electroneutrality model had difficulty in the non-linear regime because it is a two-parameter model. The predictions made by this model are obtained by using the SMA equilibrium equations while setting the SMA steric factor σ_i to zero. As the degree of non-linearity increases, the SDM/electroneutrality predictions diverge dramatically from the experimental data in Fig. A1b.

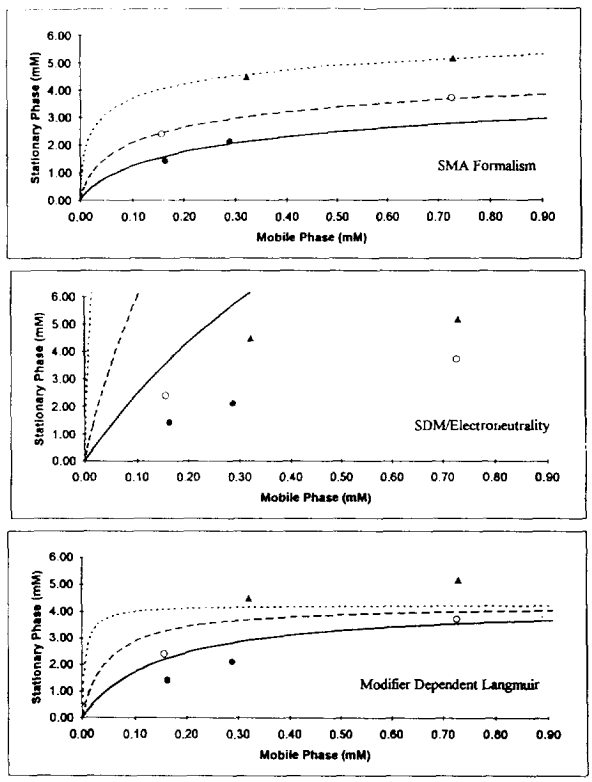

Fig. A1. Isotherms of cytochrome c on a strong cation-exchange column at pH 6.0. The experimental data was collected at (▲) 90, (○) 125 and (●) 150 mM sodium. The predictions of the three isotherms are depicted at 90 mM (dotted line), 125 mM (dashed line) and 150 mM (solid line) sodium.

In order to fit the model of Antia and Horváth, using two parameters to fit the infinite dilution data (as Antia and Horváth suggest), Z_i is chosen equal to the characteristic charge within the SMA formalism and a_i is set equal to the group of SMA parameters: $K_{1i}\Lambda^{\nu_i}$. Finally, λ_i is estimated by minimizing the sum of squares error between the values Q_i obtained in non-linear frontal experiments and the model's estimates of those values. In preparing Fig. A1c, λ_i was selected to be 4.3. Examining the figure, while substantially better than SDM/electroneutrality, this model is inferior to SMA in its ability to predict non-linear protein adsorption. This formalism has the additional disadvantage of

being unable to account for induced salt gradients in displacement chromatography. Hence it is wholly inadequate to account for the behavior of proteins in displacement chromatography [13].

More extensive tests of the ability of SMA to predict isotherms of proteins and polyelectrolytes across a range of salt have already been conducted [15–19].

References

[1] F.G. Helfferich and P.W. Carr, *J. Chromatogr.*, 629 (1993) 97.

[2] J.C. Bellot and J.S. Condoret, *Process Biochem.*, 28 (1993) 365.

[3] H. Rhee, R. Aris and N.R. Amundson, *First-Order Partial Differential Equations: Vol. I, Theory and Application of Single Equations*, Prentice-Hall, Englewood Cliffs, NJ, 1986.

[4] H. Rhee, R. Aris, and N.R. Amundson, *First-Order Partial Differential Equations: Vol. II, Theory and Application of Hyperbolic Systems of Quasilinear Equations*, Prentice-Hall, Englewood Cliffs, NJ, 1989.

[5] N.K. Boardman and S.M. Partridge, *Biochem. J.*, 59 (1955) 543.

[6] W. Kopaciewicz, M.A. Rounds, J. Fausnaugh and F.E. Regnier, *J. Chromatogr.*, 266 (1983) 3.

[7] R.R. Drager and F.E. Regnier, *J. Chromatogr.*, 359 (1986) 147.

[8] A. Velayudhan and C. Horváth, *J. Chromatogr.*, 443 (1988) 13.

[9] P. Cysewski, A. Jaulmes, R. Lemque, B. Sebille, C. Vidal-Madjar and G. Jilge, *J. Chromatogr.*, 548 (1991) 61.

[10] A. Velayudhan and C. Horváth, *J. Chromatogr. A*, 663 (1994) 1.

[11] J.C. Bellot and J.S. Condoret, *J. Chromatogr.*, 484 (1993) 1.

[12] A. Velayudhan, *Doctoral Dissertation*, Yale University, New Haven, CT, 1990.

[13] C.A. Brooks and S.M. Cramer, *AIChE J.*, 38 (1992) 1969.

[14] A.L. Myers, *AIChE J.*, 29 (1983) 691.

[15] S.D. Gadam, G. Jayaraman and S.M. Cramer, *J. Chromatogr.*, 630 (1993) 37.

[16] J.A. Gerstner and S.M. Cramer, *Biotechnol. Prog.* 8 (1992) 540.

[17] J.A. Gerstner and S.M. Cramer, *BioPharm* 5 (1992) 42.

[18] G. Jayaraman, S.D. Gadam and S.M. Cramer, *J. Chromatogr.*, 630 (1993) 53.

[19] S.D. Gadam, S.R. Gallant and S.M. Cramer, *AIChE J.*, in press.

[20] P.C. Wankat, *Rate-Controlled Separations*, Elsevier, London, 1990.

[21] P.K. de Bokx, P.C. Baarslag and H.P. Urbach, *J. Chromatogr.*, 594 (1992) 9.

[22] C.A. Brooks and S.M. Cramer, *Chem. Eng. Sci.*, in press.

[23] J.A. Jonsson and P. Lovkvist, *Chemometrics*, 5 (1989) 303.

[24] E.V. Dose, S. Jacobson and G. Guiochon, *Anal. Chem.*, 63 (1991) 833.

[25] F. D. Antia and C. Horváth, *J. Chromatogr.*, 484 (1989) 1.